lajss.org© Latin American Journal of Solids and Structures

www.lajss.org

Nonlinear Structural Dynamics of Folding Wingtip: A Flexible Multibody Approach

Leonardo Barros da Luz[a]*, Flávio Luiz Cardoso-Ribeiro[a], Pedro Paglione[a]

[a] Dept. of Flight Mechanics, Instituto Tecnológico de Aeronáutica, São Paulo/São José dos Campos, Brazil.
Email: leobdl.formula@gmail.com, flaviocr@ita.br, pedro.paglione@gmail.com

* Corresponding author

https://doi.org/10.1590/1679-7825/e9100

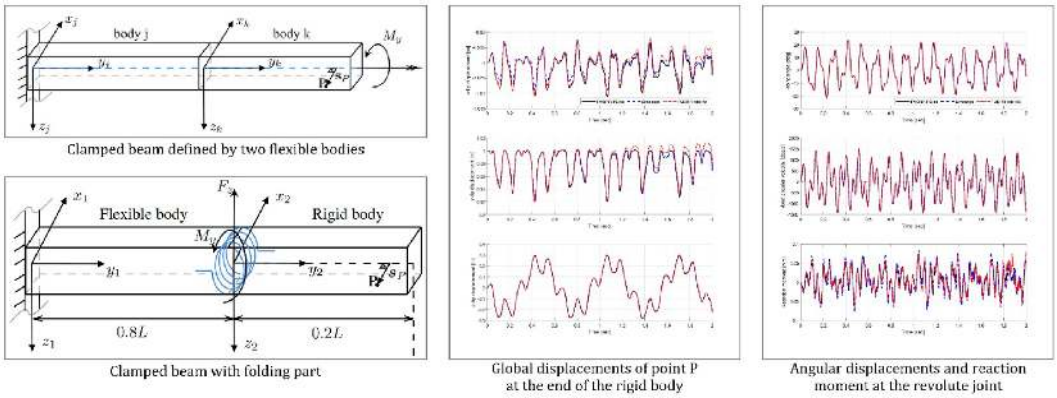
Abstract

Folding wingtips (FWTs) offer an innovative solution to reconcile aerodynamic efficiency gains of higher aspect ratio wings with airport gate restrictions. Analyzing these adaptive structures requires modeling geometric nonlinearities induced by large displacements, which traditional linear models fail to capture. This study expands the computationally efficient Flexible Multibody Rayleigh-Ritz (FMBRR) framework to analyze highly flexible structures with articulated parts. The methodology couples a linear structural model for local deformation with flexible multibody dynamics to capture global geometric nonlinearities through rigid connections. Novel contributions of this work include a torsional formulation and revolute-joint constraints specifically developed to model the FWT. Results for a highly flexible cantilever beam and an articulated structure demonstrate that the FMBRR framework accurately predicts static and dynamic nonlinear behaviors, significantly reducing computational costs compared to fully nonlinear models without losing fidelity.

Keywords

Flexible multibody dynamics, Rayleigh-Ritz method, Geometric nonlinearities, Folding wingtips, Highly flexible structures

Graphical abstract



Received April 28, 2026. In revised form June 15, 2026. Accepted August 21, 2026. Available online August 26, 2026.
https://doi.org/10.1590/1679-7825/e9100

Latin American Journal of Solids and Structures. ISSN 1679-7825. Copyright © **2026**. This is an Open Access article distributed under the terms of the Creative Commons Attribution License, which permits unrestricted use, distribution, and reproduction in any medium, provided the original work is properly cited.

1 INTRODUCTION

The continuous pursuit of greater efficiency in commercial aviation has driven the development of aircraft with higher aspect ratio wings. This design approach aims to reduce induced drag, which directly translates into lower fuel consumption and, consequently, a decrease in pollutant emissions. However, the increased wingspan imposes significant operational challenges, as many existing airport infrastructures are not compatible with large-span aircraft, restricting their operations. As a solution to this limitation, Folding Wing-Tips (FWTs) have emerged as a promising technology. They allow for the retraction of the wingtips on the ground, ensuring compatibility with gates and taxiways, and offer potential for in-flight applications, such as gust load alleviation systems and wing configuration optimization for different flight phases, as discussed in Ajaj (2020).

The main challenge in analyzing such aircraft lies in the accurate modeling of geometric nonlinearities arising from large displacements and rotations, characteristic of highly flexible structures. Traditional linear models, such as those analyzed by Guimarães Neto et al. (2017), fail to accurately capture these effects as wing flexibility increases. The articulation of the FWT introduces additional nonlinearities into the system's dynamics, which are crucial for predicting aeroelastic behavior. Although fully nonlinear Finite Element Models (FEM) or nonlinear beam models can represent this complexity, their high computational cost often makes them impractical for design and optimization phases (Su, 2008; Brown, 2003; Shearer, 2006).

The academic literature has explored various methodologies to address this challenge. Studies such as those by Castrichini et al. (2017) have used multibody dynamics with lumped-mass models. More recent approaches, like that of Esteban (2020), have demonstrated the effectiveness of combining linear finite element models with multibody dynamics to capture nonlinear effects. Other researchers, such as Kruger (2007) and Zhao and Ren (2011), have focused on simulating flexible behavior by coupling rigid beam segments with equivalent joints and springs. More recently, research has concentrated on experimental validation and the development of control strategies, both passive strategies, based on joint stiffness, and active strategies, using actuators for load alleviation and maneuvering (Healy et al., 2023; Balatti et al., 2023; Ahmadi et al., 2025).

To overcome the dichotomy between fidelity and computational cost, this work proposes a linear structural model coupled with a multibody called Flexible Multibody Rayleigh-Ritz (FMBRR), initially presented in da Luz et al. (2024). This methodology combines a linear structural model, based on the Rayleigh-Ritz method to describe the local deformation of each body, with flexible multibody dynamics. The global geometric nonlinearities, resulting from large displacements, are modeled through constraint equations that define the connections between the multiple flexible bodies that make up the complete structure. This hybrid approach offers a robust and lower-cost computational alternative compared to fully nonlinear methods, while maintaining fidelity in capturing nonlinear dynamic behavior.

While the fundamental FMBRR framework was initially introduced in da Luz et al. (2024) focusing primarily on planar bending, the present study significantly expands and corrects the methodology. The novel methodological contributions of this manuscript are threefold: First, it introduces a comprehensive structural formulation that incorporates torsion through the development of Essential Boundary Condition Polynomial Shape Functions (EPSF). Second, it presents a fundamental correction in the kinematic modeling of the structural connections. Whereas the preliminary work relied directly on Euler angles for constraint definitions—which inherently introduced numerical inaccuracies—this study formulates robust revolute-joint constraints using local reference frames and unit vectors. Finally, this enhanced and mathematically rigorous framework is directly applied to the complex 3D dynamic analysis of articulated folding wingtips, demonstrating its capability and reliability for morphing aircraft applications.

The objective of this paper is, therefore, to present and validate the FMBRR framework for the structural dynamics analysis of highly flexible wings equipped with folding tips. The methodology is detailed, focusing on the constraint equations for revolute joints and the evaluation of polynomial shape function bases for the Rayleigh-Ritz method. The results are validated against reference models, demonstrating the accuracy and efficiency of the method.

The structure of the paper is as follows: Section 2 details the FMBRR methodology, covering the fundamentals of flexible multibody dynamics and the structural representation via the Rayleigh-Ritz method. Section 3 presents the model's validation with a case of a cantilever beam with a folding part. Finally, Section 4 offers the conclusions and discusses future work.

2 METHODOLOGY: THE FMBRR FRAMEWORK

Multibody dynamics modeling is based on Shabana (1997) and Shabana (2005), which uses the floating frame approach. In the floating frame of reference formulations, two sets of coordinates are used to describe the configuration of flexible bodies, one set describes the location and orientation of a selected body coordinate system, while the second set describes the deformation of the body with respect to its coordinate system.

The motion of a flexible body is represented by the translation and rotation of the body frame in relation to the inertial frame. The body frame, denoted as j, is rigidly attached to the body with its origin not necessarily coincident with the center of mass of the body. The inertial frame, denoted as i, is fixed to an initial position. To describe the vectors from the inertial frame to the body frame of the body j, the rotation matrix $\overline{A}_{j/i}$ is used, considering the conventional 3-2-1 rotation sequence.

Then, by calculating the kinetic energy of a flexible body with both flexible and rigid-body degrees of freedom one finds the equations of motion of a flexible body given by the matrix equation (Orzechowski et al., 2017),

$$\overline{M}_j \ddot{\mathbf{x}}_j = \mathbf{Q}_j, \tag{1}$$

where $\overline{M}_j$ is the generalized mass matrix, $\ddot{\mathbf{x}}_j = [\dot{\mathbf{V}}_{O,j}^T, \dot{\boldsymbol{\omega}}_j^T, \ddot{\mathbf{q}}_j^T]^T$ is the vector of translational, rotational, and flexible accelerations, and $\mathbf{Q}_j$ is the vector of generalized forces, including quadratic velocity terms, external forces, and internal structural forces.

To describe the dynamics of a multibody system, the two flexible bodies j and k, are considered. Then, as presented in Shabana (2005), the concatenation of the dynamics of the two bodies takes place

$$\underbrace{\begin{bmatrix} \overline{M}_j & \overline{0} \\ \overline{0} & \overline{M}_k \end{bmatrix}}_{\overline{M}_t} \cdot \underbrace{\begin{bmatrix} \ddot{\mathbf{x}}_j \\ \ddot{\mathbf{x}}_k \end{bmatrix}}_{\ddot{\mathbf{x}}_t} = \underbrace{\begin{bmatrix} \mathbf{Q}_{i,j} + \mathbf{Q}_{e,j} \\ \mathbf{Q}_{i,k} + \mathbf{Q}_{e,k} \end{bmatrix}}_{\mathbf{Q}_t}, \tag{2}$$

and the union of the systems occurs through a system augmented by Lagrange multipliers $\boldsymbol{\lambda}$ that contains the equation of restriction kinematics, as

$$\begin{bmatrix} \overline{M}_t & \overline{C}_x^T \\ \overline{C}_x & \overline{0} \end{bmatrix} \cdot \begin{bmatrix} \ddot{\mathbf{x}}_t \\ \boldsymbol{\lambda} \end{bmatrix} = \begin{bmatrix} \mathbf{Q}_t \\ \mathbf{Q}_x \end{bmatrix}, \tag{3}$$

where $\overline{C}_x$ denotes the constraint matrix and $\mathbf{Q}_x$ represents the vector of generalized constraint forces, derived from the constraint equations. In the context of a holonomic system, these are specified by Shabana (2005):

$$\mathbf{C}(\mathbf{x}_t, t) = \mathbf{0}, \tag{4}$$

where $\mathbf{C}(\mathbf{x}_t, t)$ constitutes the vector of linearly independent constraint functions.

Simulating multibody systems involves solving complex Differential-Algebraic Equations (DAEs), and a common method to simplify them can lead to a drift problem where the solution becomes physically inaccurate. To correct this, this study employs the Post-Stabilization (PStab) method, presented in Chin (1995) and Nada and Bayoumi (2024). Unlike traditional approaches that can be difficult to tune, PStab avoids defining additional parameters by applying corrective adjustments directly to the velocities after each integration step. This process guides the numerical solution back toward its physical constraints, ensuring the results remain physically relevant. The PStab can be integrated with ODE solvers and involves applying a corrective adjustment to the velocities post-integration process, which is given by:

$$\dot{\mathbf{x}}_{t,i}^* = \dot{\mathbf{x}}_{t,i} - \overline{C}_x^{-1}(\overline{C}_x \dot{\mathbf{x}}_{t,i} + \dot{\mathbf{C}}), \tag{5}$$

where $\dot{\mathbf{x}}_{t,i}^*$ is the corrected velocity vector at the time step i and $\dot{\mathbf{x}}_{t,i}$ is the velocity vector at the time step i. The matrix $\overline{C}_x$ is commonly not square; thus, necessitating the use of the pseudo-inverse (Nada and Bayoumi, 2024).

2.1 Rayleigh-Ritz method for Local Flexibility

The local flexibility of each structural component is modeled using the Rayleigh-Ritz method. This approach approximates the continuous elastic displacement field of a body as a linear combination of spatial shape functions multiplied by time-dependent generalized coordinates. Considering a local coordinate system where the Y-axis coincides with the elastic axis, the continuous elastic displacements can be expressed in matrix form as $\mathbf{u}(y,t) = \bar{N}(\mathbf{s}_p)\mathbf{q}(t)$, where $\mathbf{q}(t) = [\mathbf{q}_x(t)^T, \mathbf{q}_z(t)^T, \mathbf{q}_\theta(t)^T]^T$ is the vector of elastic coordinates and

$$\bar{N}(\mathbf{s}_p) = \begin{bmatrix} \mathbf{N}_x(y_p) & 0 & z_p\mathbf{N}_\theta(y_p) \\ -x_p\dfrac{\partial \mathbf{N}_x(y_p)}{\partial y} & -z_p\dfrac{\partial \mathbf{N}_z(y_p)}{\partial y} & 0 \\ 0 & \mathbf{N}_z(y_p) & -x_p\mathbf{N}_\theta(y_p) \end{bmatrix}, \tag{6}$$

where $\mathbf{s}_p = [x_p, y_p, z_p]^T$ is the position vector of any point p in the structure and $\mathbf{N}_x(y_p)$, $\mathbf{N}_z(y_p)$ and $\mathbf{N}_\theta(y_p)$ are the vectors of shape functions for bending in X-axis, bending in Z-axis and torsion in Y-axis respectively (da Luz et al., 2024).

By adopting the Euler-Bernoulli beam theory for bending and the Saint-Venant theory for uniform torsion, the total strain energy U of a flexible body of length L is formulated as (Reddy, 2017; Megson, 2016):

$$U = \frac{1}{2}\int_0^L \Big(EI_{xx}\Big(\frac{\partial^2 u_z}{\partial y^2}\Big)^2 + EI_{zz}\Big(\frac{\partial^2 u_x}{\partial y^2}\Big)^2\Big)dy + \frac{1}{2}\int_0^L GJ\Big(\frac{\partial \theta_y}{\partial y}\Big)^2 dy\,, \tag{7}$$

where E and G are the elastic and shear moduli, I_{xx} and I_{zz} are the area moments of inertia, J is the torsional constant, $u_x = \mathbf{N}_x(y)\mathbf{q}_x(t)$ and $u_z = \mathbf{N}_z(y)\mathbf{q}_z(t)$ are the bending displacements, and $\theta_y = \mathbf{N}_\theta(y)\mathbf{q}_\theta(t)$ is the twist angle. Substituting the discretized displacement field into the strain energy integral directly yields the local stiffness matrix of the body.

Furthermore, to account for energy dissipation, the classical Rayleigh damping model is employed. The damping matrix $\bar{D}$ is defined as a proportional linear combination of the generalized mass and stiffness matrices, such that $\bar{D} = \alpha\bar{M} + \beta\bar{K}$, where α and β are the mass- and stiffness-proportional damping coefficients, respectively.

The shape functions themselves are derived from an orthogonal basis of polynomial functions tailored to meet specific boundary conditions. For bending, Two Boundary Condition Polynomial Shape Functions (TPSF) are used to satisfy the clamped-beam conditions of zero displacement resulting in:

$$\mathbf{N}_z(y) = \mathbf{N}_x(y) = \begin{bmatrix} N_{1,TPSF} & N_{2,TPSF} & N_{3,TPSF} & N_{4,TPSF} & N_{5,TPSF} \end{bmatrix}, \tag{8}$$

where

$$N_{1,TPSF} = \frac{y^2}{L^2}, \tag{9}$$

$$N_{2,TPSF} = -\frac{5y^2}{L^2} + \frac{6y^3}{L^3}, \tag{10}$$

$$N_{3,TPSF} = \frac{15y^2}{L^2} - \frac{42y^3}{L^3} + \frac{28y^4}{L^4}, \tag{11}$$

$$N_{4,TPSF} = -\frac{35y^2}{L^2} + \frac{168y^3}{L^3} - \frac{252y^4}{L^4} + \frac{120y^5}{L^5}, \tag{12}$$

$$N_{5,TPSF} = \frac{70y^2}{L^2} - \frac{504y^3}{L^3} + \frac{1260y^4}{L^4} - \frac{1320y^5}{L^5} + \frac{495y^6}{L^6}, \tag{13}$$

for the first five shape functions, as presented in da Luz et al. (2024).

For torsion, a similar approach was developed here, and Essential Boundary Condition Polynomial Shape Functions (EPSF) are utilized to satisfy the clamped condition for twist, resulting in:

$$\mathbf{N}_\theta(y) = \begin{bmatrix} N_{1,EPSF} & N_{2,EPSF} & N_{3,EPSF} & N_{4,EPSF} & N_{5,EPSF} \end{bmatrix}, \tag{14}$$

where

$$N_{1,EPSF} = \frac{y}{L}, \tag{15}$$

$$N_{2,EPSF} = \frac{4y^2}{L^2} - \frac{3y}{L}, \tag{16}$$

$$N_{3,EPSF} = \frac{6y}{L} - \frac{20y^2}{L^2} + \frac{15y^3}{L^3}, \tag{17}$$

$$N_{4,EPSF} = \frac{60y^2}{L^2} - \frac{10y}{L} - \frac{105y^3}{L^3} + \frac{56y^4}{L^4}, \tag{18}$$

$$N_{5,EPSF} = \frac{15y}{L} - \frac{140y^2}{L^2} + \frac{420y^3}{L^3} - \frac{504y^4}{L^4} + \frac{210y^5}{L^5}, \tag{19}$$

for the first five shape functions.

2.2 Connections modeling

To describe the global kinematics of the flexible multibody system, the structural connections between adjacent bodies must be formulated mathematically. The constraints are handled by treating translational and rotational motions separately, ensuring compatibility between interconnected elements.

2.2.1 Rigid connections

Rigid connections are employed to model continuous segments discretized into multiple flexible bodies, enforcing full kinematic compatibility, zero relative displacement and zero relative rotation, at the connection point L between body j and body k.

The translational constraint guarantees that the connection point remains coincident for both bodies at all times. Let $\mathbf{R}^i_{O,j}$ and $\mathbf{R}^i_{O,k}$ be the global position vectors of the origins of bodies j and k relative to the inertial frame, respectively. Given the position vector of the connection point $\mathbf{s}^j_{L,j}$ and its corresponding local elastic displacement $\mathbf{u}^j_{L,j}$ on body j, the holonomic translational constraint equation is expressed as:

$$\mathbf{C}(\mathbf{x}_t, t) = \mathbf{R}^i_{O,j} + \overline{A}_{i/j}\mathbf{s}^j_{L,j} + \overline{A}_{i/j}\mathbf{u}^j_{L,j} - \mathbf{R}^i_{O,k} = \mathbf{0}, \tag{20}$$

The rotational constraint for a fully rigid connection requires that body k follows the orientation and elastic angular deformation of body j at the boundary. By defining a Local Reference Frame (LRF), denoted by the subscribed L, at the connection point and eliminating higher-order terms under the small-angle assumption, the angular velocity of the connection

frame $\boldsymbol{\omega}_L$ is governed by the rigid-body rotation and the local elastic rotation rate of body j (Guimarães Neto et al., 2016; Esteban, 2020):

$$\boldsymbol{\omega}_L = \boldsymbol{\omega}_j + \dot{\boldsymbol{\Psi}}_L + \tilde{\boldsymbol{\omega}}_j \boldsymbol{\Psi}_L \,, \tag{21}$$

where $\boldsymbol{\Psi}_L$ represents the local elastic rotation vector and $\tilde{\boldsymbol{\omega}}_j$ represents the skew-symmetric matrix of the vector $\boldsymbol{\omega}_j$. Consequently, for a perfectly rigid inter-body connection, the non-holonomic rotational constraint at the velocity level is defined as:

$$\mathbf{C}(\mathbf{x}_t, \dot{\mathbf{x}}_t, t) = \boldsymbol{\omega}_j + \dot{\boldsymbol{\Psi}}_L + \tilde{\boldsymbol{\omega}}_j \boldsymbol{\Psi}_L - \boldsymbol{\omega}_k = \mathbf{0} \,. \tag{22}$$

2.2.2 Revolute joint connections

To model articulated subcomponents, such as folding wingtips, the connection must allow a single free relative degree of freedom around a designated hinge line while constraining all other motions. For a revolute joint, the translation is locked using the same holonomic constraint defined in Eq. (20).

However, the rotational constraints are modified to allow free rotation about the hinge axis. Let $\mathbf{v}_h$ be the unit vector characterizing the axis of rotation defined in the local frame of body j at the connection point L. To complete the joint kinematics, two orthogonal unit vectors, $\mathbf{v}_a$ and $\mathbf{v}_b$, are defined on the subsequent body k perpendicular to its longitudinal axis. The restriction is enforced by ensuring that these two axes remain strictly orthogonal to the rotation axis of the hinge line throughout the motion:

$$\mathbf{C}(\mathbf{x}_t, t) = \left(\overline{A}_{i/L}\mathbf{v}_h\right)^T \overline{A}_{i/k}\mathbf{v}_a = 0 \tag{23}$$

and

$$\mathbf{C}(\mathbf{x}_t, t) = \left(\overline{A}_{i/L}\mathbf{v}_h\right)^T \overline{A}_{i/k}\mathbf{v}_b = 0 \,, \tag{24}$$

where $\overline{A}_{i/L}$ represents the transformation matrix from the local connection frame to the inertial frame. Equations (23) and (24) constitute holonomic positioning constraints for the joint. These expressions are subsequently differentiated with respect to time to derive the final kinematic constraint matrix $\overline{C}_x$ and the vector of generalized constraint forces $\mathbf{Q}_x$ for the dynamic formulation.

3 NUMERICAL RESULTS

3.1 Highly flexible cantilever beam

To verify the proposed FMBRR framework, particularly its novel torsional formulation, the static and dynamic behaviors of a highly flexible cantilever beam are analyzed. This base model extends the bending verification previously presented in da Luz et al. (2024). The physical system consists of a clamped beam subjected to a torsional moment, M_y, at the free end, disregarding damping and gravitational effects, as illustrated in Figure 1. The structural properties of the beam are summarized in Table 1.

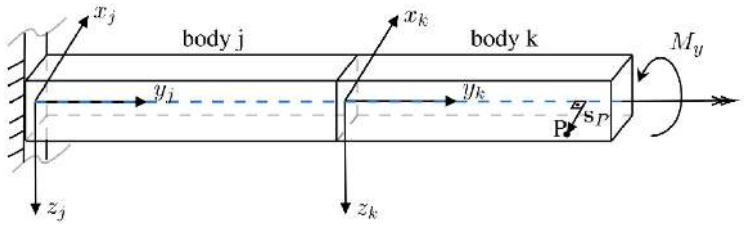


Figure 1: Clamped beam defined by two bodies j and k with a M_y moment at the free end.

Table 1. Beam Properties.

Properties	Value	Units
Length	1.0	m
Torsional Stiffness	50	N m^2
Flat Bending Stiffness	50	N·m^2
In-plane Bending Stiffness	1000	N·m^2
Mass per length	0.2	kg/m
Flat Bending Inertia per length	1E-6	kg·m
Rotational Inertia per length	1E-4	kg·m
In-plane Bending Inertia per length	1E-4	kg·m

3.1.1 Discretization strategy and validation setup

In the FMBRR approach, the continuous beam is discretized into a finite number of interconnected flexible segments (bodies). While the local deformation of each body is modeled linearly using the Rayleigh-Ritz method, the global geometric nonlinearities are captured through the kinematic constraint equations at the connections between these bodies. The specific number of bodies and shape functions are varied in the subsequent static and dynamic analyses to evaluate the method's convergence and accuracy.

To validate the FMBRR results, two established nonlinear structural dynamics codes are employed as references:

- **Aeroflex**: A strain-based geometrically nonlinear structural code (Ribeiro et al., 2012; Ribeiro, 2018). For this validation, the Aeroflex model was discretized using 10 elements to ensure a converged high-fidelity reference. It is used as the baseline for both static and dynamic comparisons.
- **MATLAB Simscape Multibody**: A commercial multibody dynamics software. The Simscape model was discretized using 4 rigidly connected flexible bodies, which was determined to be sufficient to capture the dynamic response within the software's formulation. It is used as the baseline only for dynamic comparisons.

The difference in discretization between the reference models stems from their inherent numerical characteristics: Aeroflex requires 10 elements to guarantee a strictly converged, high-fidelity structural baseline, while 4 bodies proved sufficient for Simscape to capture the macroscopic dynamic response within its specific multibody formulation without incurring excessive computational costs.

For all dynamic simulations, the systems of equations are integrated using MATLAB's ode15s solver. The primary metric for comparison across all models is the global displacement of point P, located at the free end of the beam and defined by the unit vector $\mathbf{s}_P = [1,0,0]^T$.

3.1.2 Static results

To establish the appropriate discretization for the FMBRR framework, an initial convergence study was conducted by varying the number of bodies from 2 to 10 and the number of shape functions from 2 to 5. Because the method is limited by the small local displacement condition within each flexible body, the required discretization is inherently linked to the maximum applied load. This preliminary analysis determined that simulating the target maximum torsional moment of 45 Nm strictly requires a 10-body discretization to prevent the internal deformations from violating the linear formulation limits. Additionally, utilizing 5 shape functions per body was adopted as it provided a robust and reasonable margin to guarantee local convergence.

Having established the 10-body configuration with 5 shape functions as the valid baseline for the maximum expected load, this single discretized model was utilized to calculate the static equilibrium for the entire range of applied moments, $M_y = [5,10,15,20,25,30,35,40,45]$. To evaluate the accuracy of the proposed framework under varying load magnitudes, the global tip displacements predicted by this 10-body FMBRR model were directly compared against the high-fidelity Aeroflex reference model evaluated under the exact same load configurations.

Figure 2 presents a comparative analysis of FMBRR model against reference standards for beam tip deflections in the Z and X axes. The EPSF base exhibited results closely aligning with the reference standards. Moreover, it is noted that the FMBRR framework approximates the curve in the Z-axis with higher accuracy than in the X-axis. This divergence occurs because the local structural model, based on the Rayleigh-Ritz method, is strictly linear and thus does not account for the longitudinal foreshortening caused by transverse bending. Consequently, the displacement in the X-axis is an exclusive effect of the global multibody kinematics, captured solely through the finite rotations of the local reference frames at the connection joints. Therefore, while the Z-axis displacement benefits from both the local shape functions and the global rigid-body rotations, the accuracy of the X-axis displacement relies heavily on the discretization level (number of bodies).

Additionally, Figure 3 shows the maximum local rotation, demonstrating that it consistently remained near or below 5°. This threshold provides a mathematical justification for maintaining the assumption of small local displacements. The linear structural model formulation relies on small-angle approximations. For a local rotation of 5°, approximately 0.087 radians, the error in the sine approximation is less than 0.2%, and the cosine value remains 0.996, an error of less than 0.4%. This explicitly demonstrates that the 10-body discretization ensures the linear elastic assumption remains valid and physically consistent throughout all static simulations.

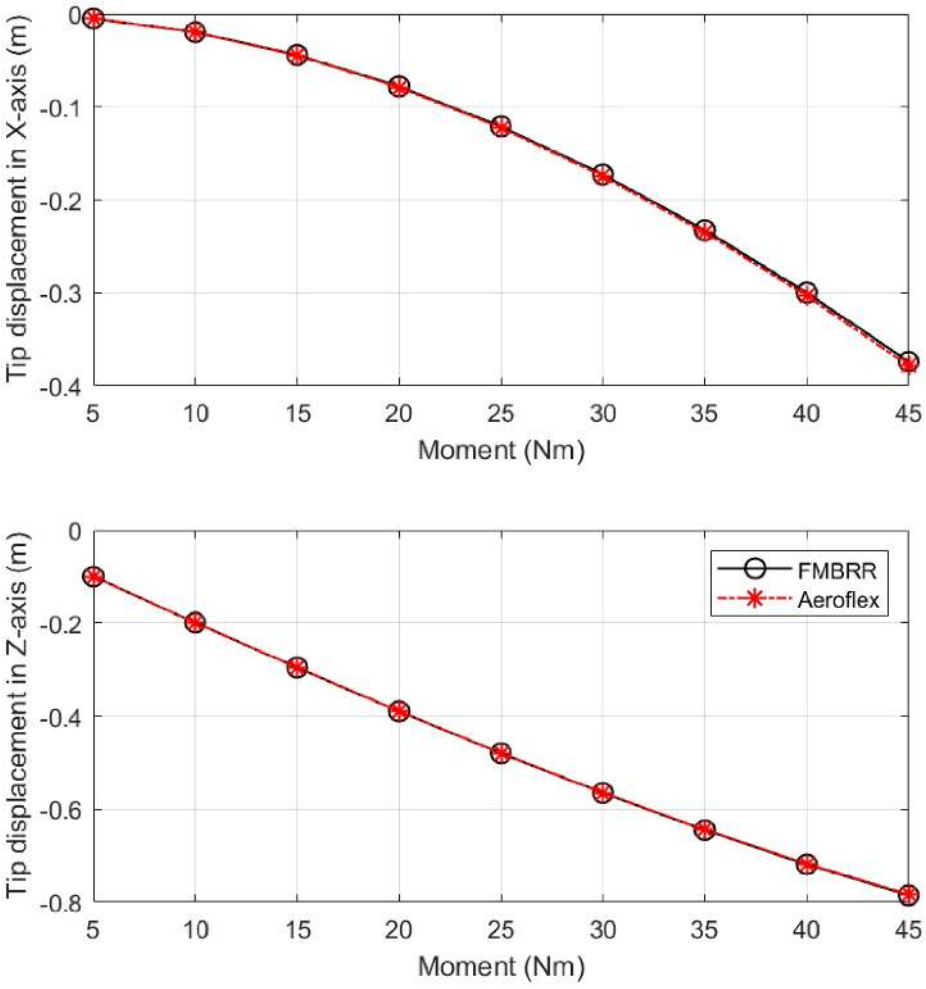


Figure 2: Comparison of global beam tip deflections in the Z-axis and X-axis as a function of the applied moment.

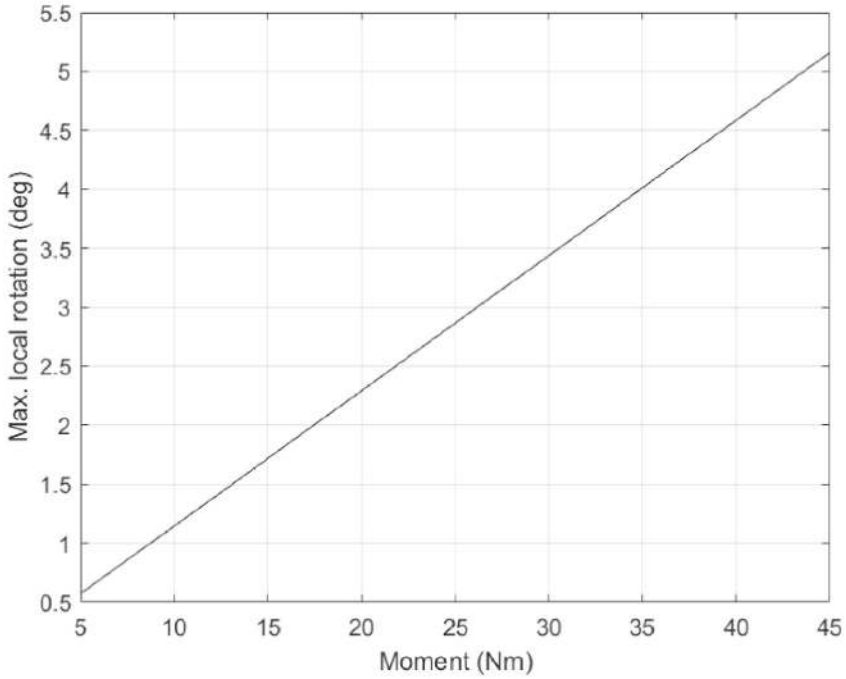


Figure 3: Maximum local rotation as function of the applied moment.

3.1.3 Dynamic results

The dynamic behavior was evaluated using four excitation cases:

Case 1: $M_y = 5\sin(10t)$;

Case 2: $M_y = 5\sin(20t)$;

Case 3: $M_y = 15\sin(10t)$;

Case 4: $M_y = 15\sin(20t)$;

In the first two cases, we have an excitation with a maximum amplitude of 5 Nm which, based on the static result, provides a maximum global deflection in the Z-axis close to 10% and for the last two cases, a maximum amplitude of 15 Nm which provides a maximum global deflection in the Z-axis close to 30%. Because the maximum excitation amplitude in the dynamic scenarios is limited to 15 Nm, the highly refined 10-body discretization is not required to maintain the small local displacement assumption. Based on the preceding static convergence analysis, a reduced FMBRR model utilizing 4 bodies and 5 shape functions is mathematically sufficient to accurately describe the structure's dynamic behavior for this specific load range without violating the local linear limits, thereby maximizing computational efficiency.

As a metric to measure the difference between the references and the models, the Normalized Residual Mean Square Difference (NRMSD) was used, defined by:

$$NRMSD = \frac{\sqrt{\frac{1}{N}\sum_{i=1}^{N}(y_{ref,i} - y_i)^2}}{y_{max} - y_{min}}, \tag{25}$$

Where y_i is the value of the vector at position i, $y_{ref,i}$ is the value of the reference vector at position i, y_{max} is the maximum value of the vector $\mathbf{y}$ and y_{min} is the minimum value.

In Table 2, the NRMSD values as percentages for both reference models and both displacement axes are presented. Upon analysis, it becomes apparent that the observed differences were more pronounced in the X-axis displacement, as previously noted in the static result discussion. Furthermore, it is clear that FMBRR closely approximates the reference results.

Table 2. NRMSD values in percentage for the global deflection of the beam tip in the Z and X axes.

Case	Aeroflex		Simscape	
	Z-axis	X-axis	Z-axis	X-axis
Case 1	4.1	0.36	4.09	0.34
Case 2	4.51	0.71	4.46	0.67
Case 3	4.03	0.36	4.02	0.35
Case 4	4.45	0.71	4.40	0.69

Figure 4 and Figure 5 show the global displacements at the beam tip for FMBRR, Aeroflex, and Simscape. Upon examination of the results, it is evident that FMBRR consistently approximates the reference results throughout the entire time interval under study. Furthermore, in Table 3, it can be observed that the FMBRR has the lowest computational cost compared to the references.

Table 3. Comparison of computational cost for Case 4: $M_y = 15\sin(20t)$.

Model	Simulation time (s)	Computational time (s)
Aeroflex	1.0	770.00
Simscape	1.0	751.08
FMBRR	1.0	183.95

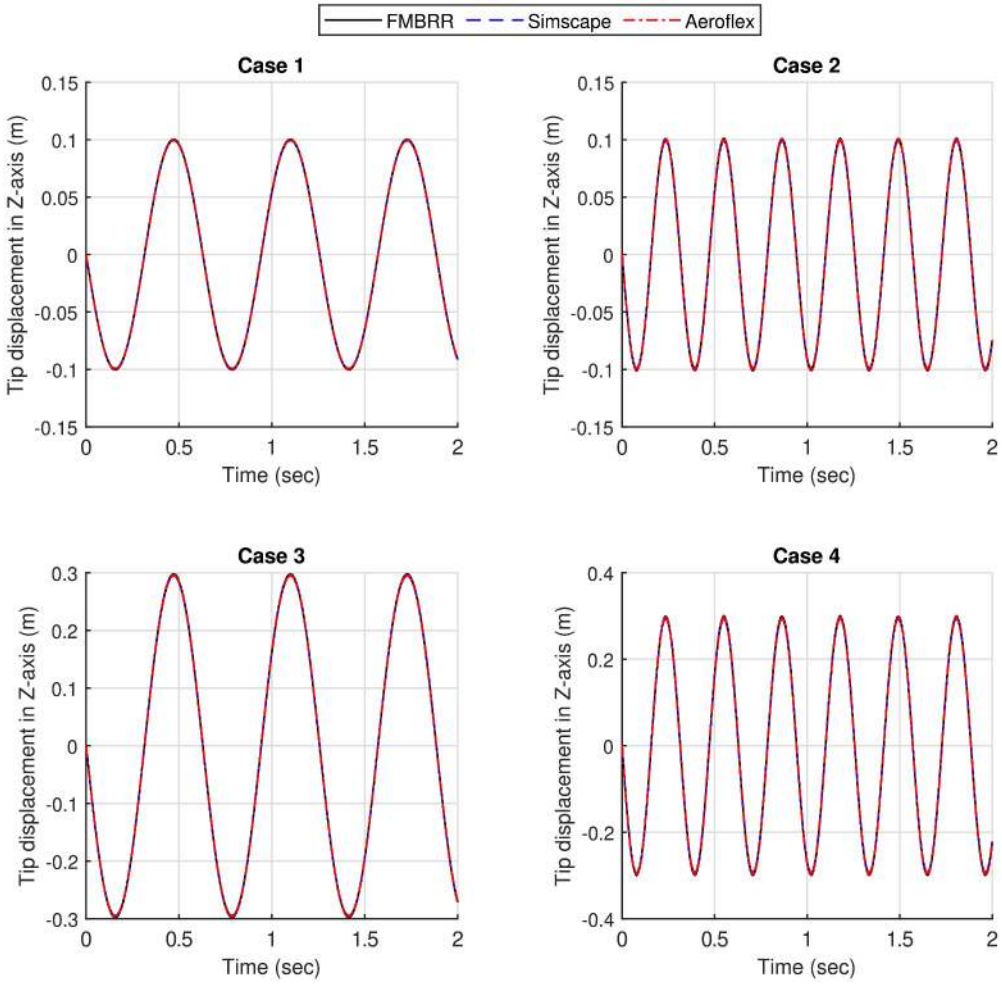


Figure 4: Global beam tip deflections in the Z-axis as a function of time.

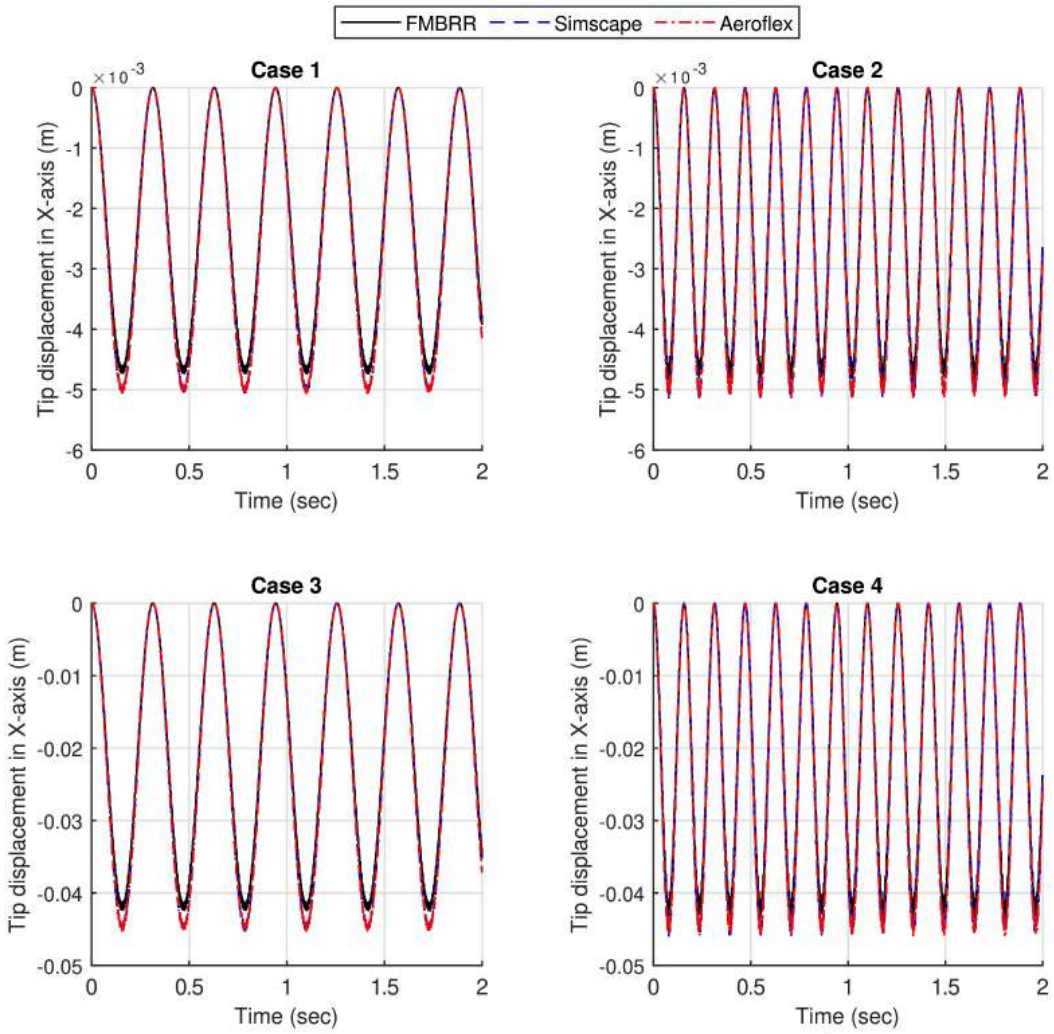


Figure 5: Global beam tip deflections in the X-axis as a function of time.

3.2 Highly flexible cantilever beam with folding part

To validate the implementation and modeling of the rotational constraints, the same beam from Subsection 3.1 was employed. The configuration consists of a rigid body, defining a folding part, which constitutes 20% of the beam's total length. The remaining 80% is a flexible body, to which the folding part is attached via a revolute joint. To induce dynamic motion, a time-varying vertical force, F_z, and moment, M_y, were applied, in addition to a spring at the connection. As illustrated in Figure 6, this setup serves as a representative abstraction of a folding wingtip system, consisting of a highly flexible inner wing coupled to an articulated rigid tip. This architecture is characteristic of FWT designs aimed at gust load alleviation. To evaluate the framework's robustness, the applied time-varying loads mimic transient in-flight aerodynamic excitations. Furthermore, gravitational forces were included, while structural damping was intentionally neglected to isolate the geometric nonlinearities and rigorously test the multibody kinematic constraints.

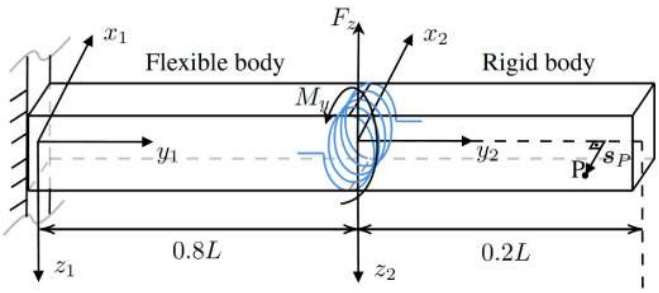


Figure 6: Clamped beam with folding part.

As a reference model, Simscape was utilized again. The reference model was configured with four rigidly connected flexible bodies and a single rigid body attached to the extremity of the final flexible body through a revolute joint. Figure 7 displays the block diagram used to define the problem in Simscape.

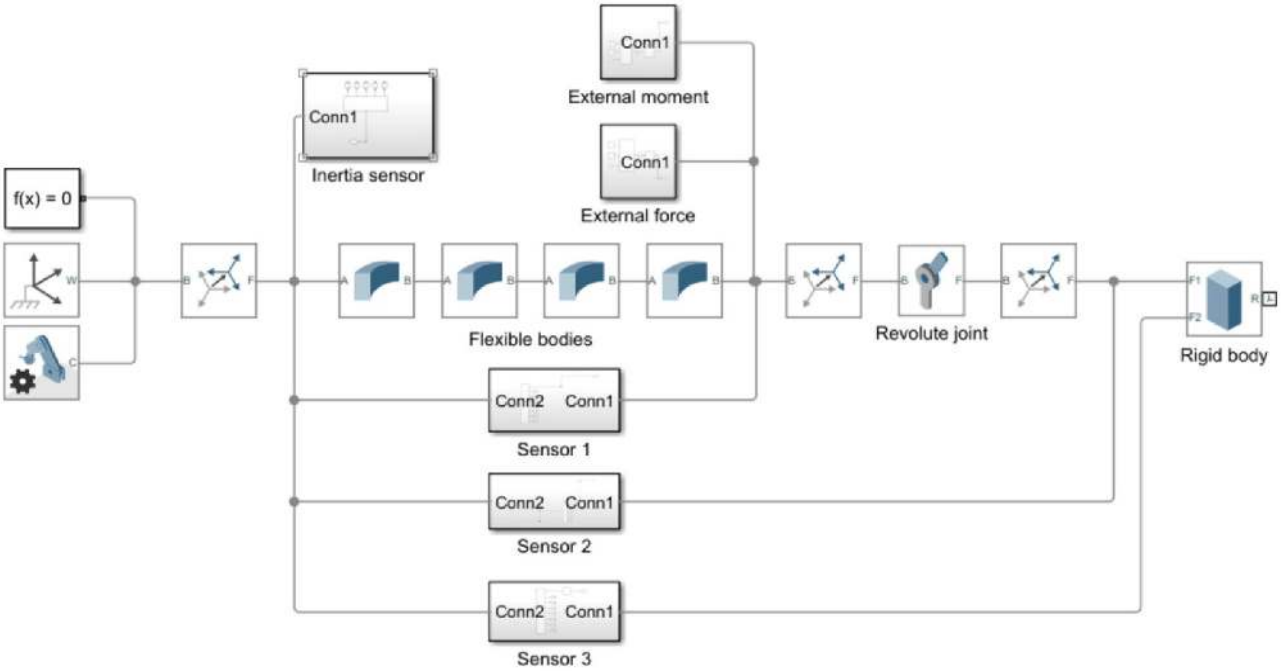


Figure 7: Simscape diagram for the clamped beam with a folding part.

The global displacements of point P, defined by the unit vector $\mathbf{s}_P = [1,0,0]^T$ at the end of the rigid body, were used as metrics for comparison between the reference and the FMBRR models. The applied force was defined as $F_z = 70\sin(10t)$ and the moment as $M_y = 7\sin(10t)$, with a spring constant of $k = 0.05$ Nm/deg.

Two simulations were executed: the first, designated FMBRR-ode15s, utilized the ode15s solver without the PStab method. The second, FMBRR-PStab, incorporated the PStab method. The results are presented in Figures 8 and 9.

Analysis of the results in Figure 8 reveals the presence of the numerical drift phenomenon in the FMBRR-ode15s simulation. Because the flexible multibody equations of motion are formulated as Differential-Algebraic Equations (DAEs), standard numerical integration algorithms evaluate the unconstrained accelerations. Over time, small truncation errors accumulate during the integration process, leading to a progressive violation of the kinematic constraints at the position and velocity levels. This drift clearly causes a divergence in the X and Y-axis tip displacements when compared to the Simscape results. Consequently, these results indicate that stabilization is necessary to maintain constraint consistency in long-term dynamic simulations of articulated structures. This was successfully resolved in the FMBRR-PStab simulation, which projects the state variables back onto the constraint manifold at each time step, yielding global displacements in excellent agreement with the high-fidelity reference.

Furthermore, examination of Figure 9 makes it evident that the model accurately captures the highly nonlinear dynamics of the revolute joint connection. The joint angle exhibits large finite rotations, oscillating between -20° and +25°. This extreme angular variation clearly validates the robustness of the unit-vector-based constraint formulation, proving its capability to handle large spatial rotations without encountering the mathematical singularities typically associated with Euler angles. Additionally, the reaction moment at the joint, obtained via Lagrange multipliers, shows excellent correlation with the values obtained from Simscape. The presence of high-frequency oscillatory components in the reaction moment plot highlights the framework's capability to accurately resolve the complex dynamic coupling between the high-frequency elastic vibrations of the flexible inner wing and the rigid-body motion of the folding tip.

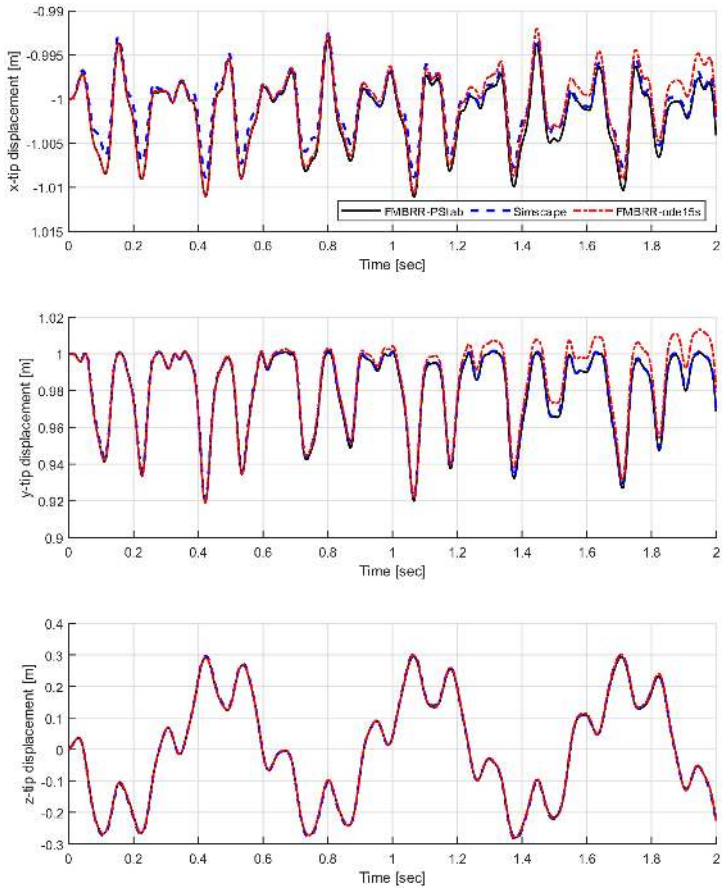


Figure 8: Comparison of the global displacements of point P at the end of the rigid body.

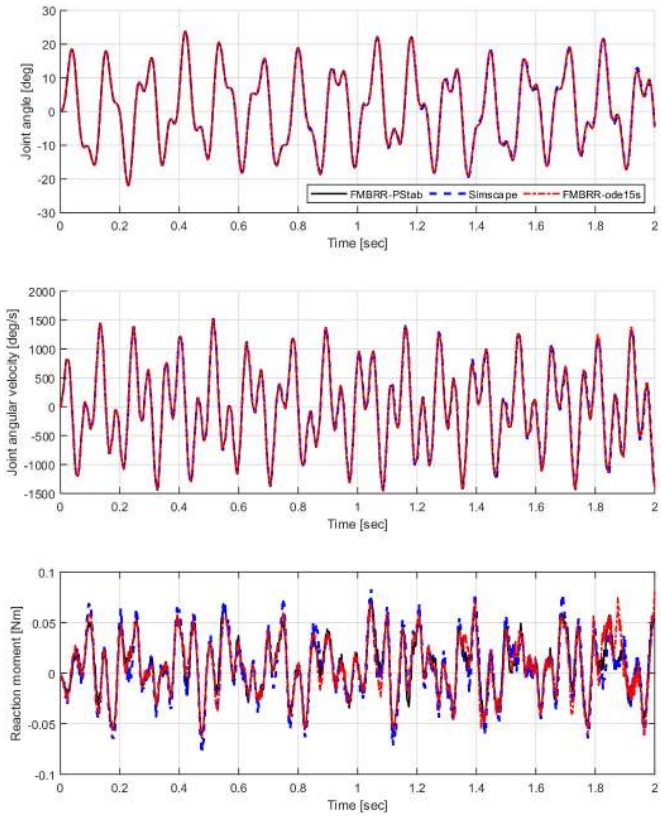


Figure 9: Comparison of angular displacements and reaction moment at the revolute joint.

4 CONCLUSION

This paper presented the development and validation of the FMBRR framework, a novel approach for analyzing the nonlinear structural dynamics of highly flexible structures with articulated parts, such as folding wingtips. The methodology successfully combines the strengths of flexible multibody dynamics to capture global geometric nonlinearities with the Rayleigh-Ritz method to model local structural deformations linearly. This hybrid formulation provides a valuable alternative that circumvents the complexity and, most notably, the high computational expense associated with fully nonlinear structural models.

The validation process demonstrated the framework's accuracy, robustness, and computational efficiency. Through rigorous comparisons with the established codes Aeroflex and MATLAB® Simscape, it was shown that the FMBRR model accurately predicts the static and dynamic behavior of highly flexible beams. Critically, the results revealed that the FMBRR framework is significantly more computationally efficient, achieving a fourfold reduction in simulation time compared to the benchmark models for the analyzed cases, without a loss of fidelity.

Furthermore, the analysis of a cantilever beam with a revolute joint successfully validated the formulation for articulated structures. This case highlighted the model's capability to handle complex connections and underscored the necessity of numerical stabilization techniques, such as the PStab method, to ensure a physically consistent solution.

In summary, the FMBRR framework stands as a reliable and computationally powerful alternative for the preliminary design and dynamic analysis of morphing aircraft. Its versatility allows for the straightforward modeling of complex, interconnected systems, and its superior computational performance makes it an exceptionally valuable tool for aerospace engineering challenges where flexibility and large deformations are critical, particularly in design and optimization phases that require numerous simulations.

Future work will focus on expanding the framework's capabilities by integrating it with aerodynamic models to conduct comprehensive aeroelastic and flight dynamics simulations. This will enable the investigation of the influence of FWTs on aircraft stability and control, as well as the development and testing of passive and active control laws for gust load alleviation and maneuver enhancement.

Acknowledgments

This study was financed in part by the Coordenação de Aperfeiçoamento de Pessoal de Nível Superior – Brasil (CAPES) – Finance Code 001. This work was also funded by Finep and Embraer S.A. under the research project Advanced Studies in Flight Physics and Control – contract no. 01.22.0552.00.

Author's Contributions: Conceptualization, LB da Luz, FL Cardoso-Ribeiro and P Paglione; Methodology, LB da Luz; Investigation, LB da Luz; Writing - original draft, LB da Luz; Writing - review & editing, LB da Luz, FL Cardoso-Ribeiro and P Paglione; Funding acquisition, FL Cardoso-Ribeiro; Resources, FL Cardoso-Ribeiro; Supervision, FL Cardoso-Ribeiro and P Paglione.

Data availability statement: Research data is only available upon request.

Editor: Elcio Cassimiro Alves e João Victor Fragoso Dias.

References

Ahmadi, M., Ellis, J., Farsadi, T., Jiffri, S., Khodaparast, H. H., & Friswell, M. I. (2025). Experimental active gust load alleviation via an actuated wingtip. In AIAA SCITECH 2025 Forum.

Ajaj, R. M. (2020). Flight dynamics of transport aircraft equipped with flared-hinge folding wingtips. Journal of Aircraft, pp. 1-13.

Balatti, D., Ellis, J., Jiffri, S., Khodaparast, H. H., & Friswell, M. I. (2023). Active hinged wingtip for gust load alleviation and manoeuvres. In AIAA SCITECH 2023 Forum.

Brown, E. L. (2003). Integrated Strain Actuation In Aircraft With Highly Flexible Composite Wings. Dissertation for a doctoral degree, Massachusetts Institute of Technology, Cambridge, Massachusetts.

Castrichini, A., Siddaramaiah, V. H., Calderon, D., Cooper, J., Wilson, T., & Lemmens, Y. (2017). Preliminary investigation of use of flexible folding wing tips for static and dynamic load alleviation. Aeronautical Journal, vol. 121, n. 1235, pp. 73-94.

Chin, H. S. (1995). Stabilization Methods for Simulation of Constrained Multibody Dynamics. Dissertation for a doctoral degree, University of British Columbia, Vancouver, Canada.

da Luz, L. B., Cardoso-Ribeiro, F. L., & Paglione, P. (2024). Rayleigh-ritz method with multibody dynamics for highly flexible structures. In The International Forum on Aeroelasticity and Structural Dynamics, The Hague, Netherlands.

Esteban, Á. C. (2020). A Geometrically Nonlinear Approach for the Aeroelastic Analysis of Commercial Transport Aircraft. Dissertation for a doctoral degree, Imperial College London, London, England.

Guimarães Neto, A. B., Silva, R. G. A., & Paglione, P. (2016). Formulation of the flight dynamics of flexible aircraft using general body axes. AIAA Journal, 54(11), 3516–3534.

Guimarães Neto, A. B., Silvestre, F. J., Cardoso-Ribeiro, F. L., Bussamra, F. L. S., Silva, R. G. A., & Cesnik, C. E. S. (2017). Validity of the assumption of small deformations in aircraft with different levels of structural flexibility. In The International Forum on Aeroelasticity and Structural Dynamics, pp. 80, Como, Italy.

Healy, F., Cheung, R., Rezgui, D., Cooper, J., Wilson, T., & Castrichini, A. (2023). Experimental and numerical nonlinear stability analysis of wings incorporating flared folding wingtips. Journal of Aircraft, vol. 60, n. 4, pp. 984-998.

Kruger, W. R. (2007). Multibody dynamics for the coupling of aeroelasticity and flight mechanics of highly flexible structures. In Stockholm: International Forum on Aeroelasticity and Structural Dynamics.

Megson, T. H. G. (2016). Aircraft structures for engineering students. Oxford: Butterworth-Heinemann, 4th ed.

Nada, A., & Bayoumi, M. (2024). Development of a constraint stabilization method of multibody systems based on fuzzy logic control. Multibody System Dynamics, vol. 61, pp. 233-265.

Orzechowski, G., Matikainen, M. K., & Mikkola, A. M. (2017). Inertia forces and shape integrals in the floating frame of reference formulation. Nonlinear Dynamics, vol. 88, pp. 1953-1968.

Reddy, J. N. (2017). Energy Principles and Variational Methods in Applied Mechanics. Chichester, West Sussex, UK: John Wiley & Sons Ltd, third ed. ISBN 9781119087373.

Ribeiro, F. L. C. (2018). Aeroflex. Available at: https://github.com/flavioluiz/AeroFlex

Ribeiro, F. L. C., Paglione, P., Silva, R. G. A., & Sousa, M. S. (2012). Aeroflex: a toolbox for studying the flight dynamics of highly flexible airplanes. In VII Congresso Nacional de Engenharia Mecânica.

Shabana, A. A. (1997). Flexible multibody dynamics: Review of past and recent developments. Multibody System Dynamics, vol. 1, n. 2, pp. 189-222.

Shabana, A. A. (2005). Dynamics of multibody systems. Cambridge University Press, 3rd ed.

Shearer, C. M. (2006). Coupled Nonlinear Flight Dynamics, Aeroelasticity and Control of Very Flexible Aircraft. Dissertation for a doctoral degree, The University of Michigan, Ann Arbor, Michigan.

Su, W. (2008). Coupled Nonlinear Flight Aeroelasticity and Flight Dynamics of Fully Flexible Aircraft. Dissertation for a doctoral degree, The University of Michigan, Ann Arbor, Michigan.

Zhao, Z., & Ren, G. (2011). Multibody dynamic approach of flight dynamics and nonlinear aeroelasticity of flexible aircraft. AIAA Journal, vol. 49, n. 1, pp. 41-54.